Postnatal connectomic development of inhibition in mouse barrel cortex

Anjali Gour, Kevin M. Boergens, Natalie Heike, Yunfeng Hua, Philip Laserstein, Kun Song, Moritz Helmstaedter*

Department of Connectomics, Max Planck Institute for Brain Research, Frankfurt, Germany.
*Corresponding author. Email: mh@brain.mpg.de

Brain circuits in the neocortex develop from diverse types of neurons that migrate and form synapses. Here we quantify the circuit patterns of synaptogenesis for inhibitory interneurons in the developing mouse somatosensory cortex. We studied synaptic innervation of cell bodies, apical dendrites and axon initial segments using 3D electron microscopy focusing on the first four weeks postnatally (postnatal days 5 to 28). We found that innervation of apical dendrites occurs early and specifically: target preference is already almost at adult levels at the fifth postnatal day (P5). Axons innervating cell bodies, on the other hand, gradually acquire specificity from P5 to P9 likely via synaptic overabundance followed by antispecific synapse removal. Chandelier axons show first target preference by P14 but develop full target specificity almost completely by P28, consistent with a combination of axon outgrowth and off-target synapse removal. This connectomic developmental profile reveals how inhibitory axons in mouse cortex establish brain circuitry during development.

The development of the complex architecture of dense neuronal circuits in the mammalian cortex has been of long-standing interest in neuroscience (*1–7*). Of particular interest is the formation of inhibitory circuits (*8–11*) that show a distinct pattern of synaptic target preference in the adult (*12*). While a full accounting of cortical interneuron types and their description by morphological and molecular markers is yet controversial (*13, 14*), three types of inhibitory synaptic target preference have been consistently identified in the cortical circuits (*15–21*): the innervation of cell bodies of excitatory neurons by inhibitory neurons that predominantly express parvalbumin or cholecystokinin (*17, 22–27*); the innervation of more distal dendrites by somatostatin-expressing interneurons (*22, 28*), and the innervation of axon initial segments by axo-axonic interneurons (*18, 29–37*). The synaptic target preferences of these neurons are not only identifiable by molecular specification and subsequent synaptic target analysis (*12*), but can be identified in a connectomic reconstruction by their distinct targeting properties (*38*). In spite of first insights into possible molecular mechanisms (*8, 33*), the postnatal formation of these synaptic target preferences, and the relative contribution of synapse addition or elimination (*39–41*) are still poorly understood.

Here, we made use of recent advances in high-resolution three-dimensional electron microscopy and analysis methods (*38, 42, 43*) to study the inhibitory neuronal circuitry at the level of single axons and their synapses (*40, 44, 45*) sampling the first days up to 3 weeks after the formation of intracortical inhibitory synapses. We report the analysis of thirteen 3D EM datasets acquired at postnatal days 5 to 56 from layers 4 and 2/3 of mouse cortex for an ontogenetic connectomic mapping of the inhibitory target choice during postnatal circuit development.

3D electron microscopy and reconstructions

We acquired thirteen 3D electron microscopy (EM) datasets from layers 4 and 2/3 of mouse cortex (Fig. 1, A to C) from nine animals at postnatal days (P) 5, 7, 9, 14, 28 and 56 using serial block-face scanning electron microscopy (SBEM) (*42*) at a voxel size of $11.24 \times 11.24 \times 30$ nm^3. The datasets were between 45 and 200 μm in extent per dimension, totaling a volume of 8.78 million μm^3 [see table S1 and Fig. 1C; note that the P28 and P56 datasets were previously published (*38, 45*); all datasets were obtained from primary somatosensory cortex (S1) except P56 from posterior parietal cortex]. Samples were stained using an enhanced en-bloc EM protocol (*46*), and datasets were reconstructed using webKnossos (*43*). All reconstructions and synapse annotations were performed by an expert annotator [Fig. 1, D and E; see data S1 for illustration of the synapse detection criteria at the different developmental stages; these criteria were derived from those used in (*38, 44, 45, 47, 48*) and calibrated in additional high-resolution EM datasets from P7 and P9, see supplementary materials] and proofread and reannotated by a team of 6 experts with cross-validation (fig. S4 and supplementary text).

Synaptic target preference of axons in layer 4

We first identified cell bodies and apical dendrites in the datasets from P7, P9, P14, P28 (Fig. 1E), searched for synapses innervating these cell bodies and the shafts of these apical dendrites, reconstructed the presynaptic axons seeded at these synapses, identified all other output synapses of these axons, and determined the postsynaptic targets of these other synapses (Fig. 2, A to C, n = 10,432 synapses, n = 526 axons, 78.79 mm path length total). Based on these data, we computed the local connectomes (Fig. 2D), which indicated that already at P7, thus a few days after the first intracortical chemical synapses are formed, axonal target preference was present for apical dendrites and cell bodies (Fig. 2E and Table 1).

Axon initial segments were also identified and found to be innervated by P14 (no innervation at P7 and P9, Fig. 2, D and E). However, the axons innervating axon initial segments in L4 at P14 did not show preference for axon initial segment innervation, which was consistent with results from P28 (38). Rather, these axons had a preference for soma innervation and were indistinguishable from soma innervating axons (Fig. 2E).

Target preference for somata and apical dendrites

We then analyzed the time course of axonal target preference in more detail for the innervation of somata and apical dendrites in L4 (Fig. 3). For this, we measured the fraction of synapses of an axon that had been identified by its innervation of a cell body that were again innervating cell bodies, and similarly for axons identified by their innervation of an apical dendrite (Fig. 3, A to E), yielding the conditional innervation of a target B given a synapse on target A: $p(B|A)$.

Conditional reinnervation of apical dendrites [$p(AD|AD)$, Fig. 3, A and B) occurred for 31.7 ± 10.1% of synapses per axon already at P5 (n = 58 synapses, n = 7 axons), and for 14.62 ± 4.51% of synapses per axon at P7 (Fig. 3, A and B; Table 1 for statistics). This remained unchanged at P9, increased by about 60% between P9 and P14 to 25.16 ± 3.12% and remained constant until P28. Possible innervation of AD shafts by excitatory axons, which alter their preference for spine/shaft innervation over age, did not affect our conclusions (fig. S5 and supplementary text).

Conditional reinnervation of somata [$p(soma|soma)$] was almost absent at P5, where synapses onto somata were very rare, and those axons that innervated somata had low preference for soma innervation (2.9 ± 2.1%, n = 101 synapses, n = 12 axons, Fig. 3E). At P7 conditional reinnervation of somata occurred for only 6.01 ± 1.07% of synapses per axon (Fig. 3, C and D, and Table 1). Between P7 and P9, this increased 2.7-fold reaching a conditional soma reinnervation of 16.07 ± 1.46% of synapses per axon at P9 (similar results were obtained when also considering the innervation of somatic

filopodia, fig. S1). From P9 to P14, we found an additional 1.5-fold increase in target preference for somata to 23.38 ± 1.76%, with no further change at P28. Control experiments in an additional animal at P7 and at P9 confirmed the measurements of target preference (fig. S4 and supplementary text).

With this, the development of synaptic target preference was found to be different for the three investigated subcellular targets: essentially fully established axonal preference for apical dendrites already at P5 [consistent with an early impact of apical-dendrite-preferring interneurons (49)], gradual postnatal development of preference for cell bodies from almost absent somatic innervation at P5 to full preference by P14 with steepest increase between P7 and P9 (Fig. 3E), and absence of conditional preference (but preference for somata) for those axons innervating axon initial segments in L4 (see below for an analysis of axon initial segment innervation in L2/3).

Developmental establishment of synaptic target preference for somata

We next wanted to understand the possible mechanisms behind the almost 3-fold increase in innervation preference for somata between P7 and P9. Changes in the geometry of cell body distribution over age could not account for increased soma innervation from P7 to P9 (fig. S2, A and B). To distinguish between the case that the increased preference of an axon for soma innervation from P7 to P9 was based on that axon's innervation of additional cell bodies each via one synapse; or alternatively by adding multiple synapses onto the very same individual postsynaptic cell body that had already been innervated (corresponding to an increased multiplicity of innervation, Fig. 3, F and G), we calculated the average number of synapses an axon made on the same individual soma. Innervation multiplicity did not change between P7 and P9 (Table 1, Fig. 3G, and fig. S3) but increased between P9 and P28. This indicated that re-innervation of the same individual cell body was not the cause for the 3-fold increase in somatic innervation preference between P7 and P9. When analyzing the multiplicity of innervation of apical dendrites (Fig. 3H and fig. S3), we again found no difference between P7 and P9 (but possibly a slightly higher level of initial multiplicity at P7, fig. S3), but an increase of such innervation multiplicity from P9 to P14. This data indicated that the enhancement of multiple synaptic innervations of the same individual target (individual somata, individual apical dendrites) occurred primarily after P9 and was thus temporally separated from the initial establishment of subcellular target preference.

Postsynaptically, the total number of synapses received per soma (Fig. 3, I and J) increased 1.5-fold between P7 and P9, but 9.4-fold between P9 and P28 (Table 1 and Fig. 3I), thus the largest increase in total somatic input innervation

occurred after P9, i.e., after the establishment of target preference in the presynaptic soma-preferring axons.

Specific addition versus antispecific pruning of synapses

For an axon to increase the fractional innervation of a postsynaptic target, two mechanisms can be distinguished (Fig. 4A): either, "on-target" synapses could be selectively added (specific synapse addition; this includes the outgrowth of novel axonal branches with target selective synapses), or "off-target" synapses could be selectively removed (antispecific synapse pruning). Both of these mechanisms have particular collateral effects: for an axon to increase, for example, its target innervation from 10% of its synapses to 25% by specific synapse addition, newly formed synapses would have to be either highly target-selective (for example, the addition of 20% synapses with 100% target selectivity would yield a 2.5-fold preference increase, Fig. 4A) or yield a large increase in synapse number. The latter could either be implemented by axonal outgrowth, which would increase path length density per axon, or synapse density increase per axonal path length. In all of these cases, the density of synapses along the axon would either remain constant or increase.

Antispecific synapse pruning, to the contrary, would yield a decrease in axonal synapse density: in order to increase fractional synaptic target innervation from 10 to 25% by removal of off-target synapses, the density of synapses along the axonal path would have to decrease by a factor of 2.5 (Fig. 4A).

We therefore measured the density of synapses along axons for soma-targeting axons (Fig. 4B). Between P7 and P9, synapse density along axons decreased about 2-fold from 0.168 ± 0.014 synapses per micrometer axonal path length to 0.088 ± 0.006 synapses per micrometer (Table 1). Since this coincided with the about 2.7-fold increase in synaptic target preference for these axons, and could quantitatively account for a fraction of the observed effect of preference increase, we interpret this as support for antispecific synapse pruning as a mechanism contributing to target preference increases for soma-targeting axons during development. The sparsening of synapses along soma-innervating axons was also directly visible in the reconstructions (Fig. 4, C and D). During that same period, overall volume density of non-excitatory synapses stayed constant (fig. S2C), and the decrease in axonal synapse density was not observed for AD targeting axons (Fig. 4, E and F, and Table 1).

Somatic versus proximal dendritic synapses

Inhibitory axons with preference for soma innervation (50–53) are known to target not only somata, but the proximal dendrites of the postsynaptic excitatory cells (17, 22), see Fig. 2B. At P28, the fraction of synapses onto cell bodies for these axons was reported as 21% with a co-innervation of proximal dendrites of 36.8% (38). We therefore wondered whether the observed changes in axonal target preference and synapse density of soma-innervating axons were specific to axonal synapses made onto cell bodies or extended to those synapses made onto proximal postsynaptic dendrites. Proximal synapses (defined as synapses proximal to the second-order dendritic branch points along the postsynaptic cell and less than 20 μm from the postsynaptic cell's soma, Fig. 4G) were in fact not reduced in density along the presynaptic axons between P7 and P9, either (Table 1 and Fig. 4H), while synapses made onto the more distal postsynaptic dendrites were reduced in density along the presynaptic axons. Together, this suggests that proximal dendritic as well as somatic synapses are exempted from the reduction in axonal synapse density that the synapses placed more distally on the postsynaptic neuron are exposed to.

Development between P9 and P28

In AD targeting axons, the about 60% increase in target preference from P9 to P14 (Table 1 and Fig. 3B) was accompanied by an about 50% increase in synapse density, which could be consistent with addition of specific synapses (8, 54). The increased multiplicity of apical dendrite innervation from P9 to P14 (by about 40%, Fig. 3H and Table 1) could strongly contribute to this enhanced preference from P9 to P14. For soma-targeting axons, the additional 1.45-fold increase in fractional innervation preference for somata between P9 and P14 (Fig. 3D) could also be partly contributed by the increase of innervation multiplicity per somatic target (by about 30%, Fig. 3G and Table 1), thus potentially via an additional mechanism different from the initial increase in target preference between P7 and P9 in these axons.

From P14 to P28, neither for apical dendrite nor soma-targeting axons, the overall 1.7-to 1.9-fold increase in axonal synapse density (Fig. 4, B and E) was accompanied by further increases in target preference (Fig. 3, B and D).

Development of axon initial segment innervation in layer 2/3

We then turned to datasets from the supragranular layers to study the connectomic development of axo-axonic innervations targeted to the axon initial segments of pyramidal neurons in adult animals which are known to be absent in layer 4 (35, 38) and are integrated into the supragranular layers comparably late during development (35).

At P9, we observed only spurious innervation of axon initial segments (Fig. 5, A and B), these were provided by axons that otherwise innervated somata and dendrites (table S2). To characterize the axons innervating axon initial segments, we reconstructed all of these axons' output synapses (Fig. 5C) and determined whether these showed a preference for axon

initial segment innervation (Fig. 5D). At P14, a subset of axons showed enhanced preference for innervation of axon initial segments: 9.6% (5 of 52) of axons innervating axon initial segments made more than 40% of their other output synapses again onto axon initial segments (Fig. 5, A, C, and D, and Table 1). At P28, about 20% of axons innervating the axon initial segment had a high preference for such innervations: these axons made >80% of their other synapses again onto axon initial segments (Fig. 5D and Table 1). We identified axons with high preference for axon initial segment innervation as "axo-axonic" (*18*) and those with low target preference for axon initial segments as "non-AIS-preferring" (group assignment via cluster analyses, see methods). The non-AIS-preferring axons showed a preference for soma innervation and were indistinguishable from soma-preferring axons (table S2).

Synaptic composition of axon initial segment innervation between P14 and P28

We then focused on the development of axon initial segment innervation between P14 and P28 (Fig. 5, A and E). About one-third of the input synapses onto axon initial segments at P14 were from axo-axonic axons (Fig. 5E and Table 1). At P28 that fraction had increased to about 60%. This indicates that even in adolescence, the innervation of axon initial segments is not exclusively maintained by axo-axonic axons, but at least about 40% of synapses onto axon initial segments are contributed by other axons. Accordingly, when quantifying the number of axons innervating a given axon initial segment, we found an increase in both the number of axo-axonic input axons (from 1 at P14 to about 4 at P28) and non-axo-axonic axons (from about 5 at P14 to about 10 at P28), yielding an input composition of axon initial segment innervation at P28 of about 20 synapses from about 4 axo-axonic axons [consistent with (*36*)] and about 10 synapses from about 10 non-axo-axonic axons.

Since axo-axonic innervation preference developed about one week later than soma- and apical dendrite-preferences, the non-specific innervation of axon initial segments found even at P28 (Fig. 5D) could correspond to a population of developing axo-axonic axons that would mature later. To estimate this effect, we analyzed an additional 3D-EM sample from a two-month-old animal (P56) which was obtained from L2/3 of posterior parietal cortex [EM data previously published in (*45*)]. We mapped all input synapses onto an axon initial segment and found that again, at least about 40% of the input synapses were made by non-axo-axonic input axons (Fig. 5, D and E). This indicates that even in the adult, a large fraction of input synapses of axon initial segments is established by axons that otherwise have no preference for axo-axonic innervation.

Development of axo-axonic target preference

We then analyzed in more detail the development of target preference in those axons at P14 and P28 that had high preference for axon initial segment innervation. At P14, axo-axonic axons made only about 60% of their synapses onto axon initial segments (Fig. 5D and Table 1), the other synapses were primarily on dendritic shafts and spines (table S2). At P28, the fraction of synapses that axo-axonic axons made onto axon initial segments had increased to about 90%, their other 10% of synapses were made on shafts and spines, but not somata. Note that already at P14, some off-target synapses were noticeably smaller and less distinct than the AIS synapses of the same axons, possibly corresponding to gradual removal of these non-AIS synapses (Fig. 5D) (*55*).

Quantitatively, which mechanism could generate this about 1.6-fold increase in target preference in axo-axonic axons from P14 to P28 (Fig. 6, A and B)? Overall synapse density along these axons was largely constant between P14 and P28 (Table 1). The density of synapses onto axon initial segments increased by about 1.7-fold between P14 and P28 (Fig. 6C), while during the same time span, the density of off-target synapses decreased by a factor of 4.2.

Vertically oriented axon branches with several synapses onto axon initial segments ("axonal cartridges") are a morphological signature of axo-axonic axons in the adult (*18*). Since we observed no cartridges at P14 (Fig. 6A), but a higher frequency at P28 (Fig. 6B), we wondered whether the increase of target preference for axon initial segments between P14 and P28 could be fully explained by outgrowth of cartridges establishing target specific synapses (Fig. 6, D to F). To quantify the relevant parameters, we measured the density of AIS synapses along cartridges at P28 and the relative path length contributed by cartridges in axo-axonic axons at P28 (Table 1). We then computed the predicted fractional innervation of axon initial segments for axo-axonic axons at P28 under this model (Fig. 6F). In fact, this model can account for most of the enhanced innervation preference at P28 (Fig. 6F; model prediction: 76 to 81%; measured preference: 89 to 95%). In order to account for the remaining target preference, we quantified the additional pruning of off-target synapses that could contribute the remaining drop of off-target innervation from P14 to P28. With an elimination of 54 to 65% of off-target synapses, the measured innervation preference for axon initial segments would be explained.

We therefore conclude that a possible scenario for establishing the high-specificity targeting of axon initial segments by axo-axonic axons between P14 and P28 is the growth of cartridges establishing exclusively synapses onto axon initial segments together with the pruning of at least about 50% of the off-target synapses. This was further supported by an additional analysis of axo-axonic axons in a dataset from P56 (Fig. 5D): here, essentially no off-target synapses were found

in the axo-axonic axons.

We finally observed that already at P14, thus before cartridges are established, axo-axonic axons showed coordinated innervation of particular postsynaptic axon initial segments via their en-passant synapses (Fig. 6G). This is particularly noteworthy since this may indicate that the establishment of axonal cartridges (Fig. 6H) is only the second step in a developmental process which enables the choice and repetitive innervation of particular postsynaptic neurons at their axon initial segments.

Discussion

We determined the connectomic postnatal development of synaptic target preference in three main classes of inhibitory axons in cortex. We found three types of connectomic development (Fig. 7): axons with preference for apical dendrites showed high target preference already at the earliest measured time points (P5 and P7), which increased only moderately over postnatal development concurrent with an increase of innervation multiplicity between P9 and P14. Axons with preference for neuronal somata, to the contrary, had only low target preference at P7 (and almost none at P5), which increased almost 3-fold by P9. This increase was accompanied by a drop in the density of off-target synapses specifically in these axons, making antispecific synapse pruning a possible mechanism for establishing target preference in soma-preferring axons. Finally, axo-axonic axons in supragranular layers developed preference for axon initial segment innervations from P14 onwards, and our data was consistent with a combination of axonal cartridge growth and antispecific synapse pruning as the mechanism for establishing the observed axon initial segment target preference at P28. Notably, at early time points (P9, P14), more than 60% of synapses onto axon initial segments were made by axons that had no axo-axonic innervation preference, and this non-specific innervation decreased only moderately over development (to about 40% at P28 and P56).

Interpretation of connectomic snapshots as developmental trajectories

We used connectomic experiments to study the synaptic innervation patterns over postnatal development. These experiments are necessarily discontinuous, since an observation of the very same circuit over time is incompatible with the experimental approach of using fixed brain tissue. Therefore, the interpretation of the quantitative development of connectomic patterns as trajectories of similar axons must be treated with caution. In particular, it would be theoretically possible that the population of axons innervating somata at P7 is distinct from the population observed at P9, also because a fraction of interneurons has been shown to undergo cell death over this time range (11). Then, what we interpret

as developmental changes of axonal synapses could be a change of the mixture of axons innervating a target. However, we do not observe any high-soma-preference axons at P7 (Fig. 3D), and the measured distribution of preference at P9 (fig. S2D) showed no clear sign of bimodality. Moreover, this alternative explanation would imply that a large number of axons needs to be pruned or retracted, and a large number of new axons grown out over the course of 2 days. Still, since a range of molecularly identified interneurons have been reported to innervate cell bodies (17, 31), the possibility that a subgroup of the soma innervating axons belongs to a different cell type cannot be excluded. The prevalence of one of these cell types, cholecystokinin-positive interneurons (56), is comparably low in primary sensory cortex (57), and therefore this subtype may not be identifiable as a separate connectomic profile in our data.

Other synaptic targets, preference versus specificity

In a first order approximation, a large fraction of interneurons in cortex have been assigned to groups with common innervation preference. Quantitatively, however, these preferences do not constitute exclusivity of innervation. For soma preferring axons, about 15 to 25% of their synapses are placed on somata in the adult (12, 22, 38). If one includes proximal dendrites as target, about two third of output synapses of such axons are placed on these preferred targets (38). Accordingly, in our developmental analysis, an increase of preference for soma innervation from a few percent to close to 20% constitutes a strong enhancement of synaptic bias, and we could show that a possible mechanism, antispecific synapse removal, applies to both somatic and proximal dendritic synapses (Fig. 4, B, G, and H). Similarly, preference for distal dendrites corresponds to an innervation of apical dendritic trunks with about 20 to 25% of output synapses in the adult (38) and up to 40 to 50% onto other non-proximal dendritic targets (22, 38). Therefore, our finding of already about 20% target preference for apical dendrite trunks as early as P5 and P7 constitutes comparably high synaptic specialization.

Axo-axonic interneurons show above 80% synaptic bias in the adult, which is higher than in all other known interneurons, but not exclusive. These interneurons have been termed "Chandelier" neurons (32), but may constitute an inhomogeneous class (58). The finding that these axons establish early target preference (Fig. 5D) and systematic target choice (Fig. 6G) before the occurrence of cartridges may indicate a complex developmental impact of these neurons' activity. Since axon initial segments receive a significant fraction of inputs from non-axo-axonic axons (Fig. 5, A and E), the notion of a unique position of axo-axonic interneurons to control action potential generation in postsynaptic pyramidal cells may have to be interpreted with caution. While the target preference of these other innervations was comparable to soma-

preferring axons, they may constitute a specialized subgroup of interneurons (*31*).

Outlook

We used connectomic mapping to determine developmental changes in circuit properties in the cortex. With the acceleration of connectomic data acquisition and analysis (*38*), it is conceivable that such approaches can be used for targeted interventions with the developmental machinery, and yield a screening approach for circuit phenotypes of developmentally active molecular agents.

Materials and methods

Animal experiments

All experimental procedures were performed according to the law of animal experimentation issued by the German Federal Government under the supervision of local ethics committees, approved by Regierungspräsidium Darmstadt, F 126/1002, and according to the guidelines of the Max Planck Society.

The cortical tissue processing, 3D electron microscopy and dataset alignment for the P28 and P56 samples were described previously (*38, 45*). The ten samples at P5, 7, 9 and 14 were processed as follows.

Tissue preparation, staining, 3D-EM experiments

Male C57BL6 mice at P5, 7, 9 and 14 were anesthetized using isoflurane and perfused transcardially with 0.15 M sodium cacodylate buffer (pH = 7.4), followed by fixative solution (2.5% paraformaldehyde, 1.25% glutaraldehyde, 2 mM $CaCl_2$ in 0.08 M cacodylate buffer) using a syringe pump (PHD Ultra, Harvard Apparatus, USA). The flow rates of the buffer and fixative solution were 5 to 7 ml min^{-1} (P5, P7), 7 to 10 ml min^{-1} (P9), and 12 ml min^{-1} (P14), respectively. The volumes of the perfused cacodylate buffer and fixative solution were 3 and 12 ml (P5, P7), 5 and 15 ml (P9), and 8 and 20 ml (P14), respectively. The brains were kept in the skull after incising a small opening at the posterior and stored overnight in the fixative solution at 4°C. Using a stereotaxic instrument (Model 902 Dual small animal stereotaxic instrument, David Kopf instruments, USA), samples were then extracted by 1 mm biopsy punches (Integra, Miltex, USA). The hemispheres were stored in phosphate buffered saline (PBS, Sigma-Aldrich, USA) overnight at 4°C and were subsequently processed for Cytochrome oxidase staining to confirm the sample location (see supplementary methods).

En-bloc staining was performed as (*46*) with minor modifications; 3D-EM imaging was performed on a serial blockface EM (SBEM) setup [microtome courtesy of W. Denk (*42*)] using discontinuous mosaic imaging; and image alignment was either performed using global 3D relaxation of cross-

correlational shift vectors or in-plane stitching followed by cross-plane alignment; see table S1 and supplementary methods for details.

Identification and reconstruction of postsynaptic targets

The aligned data was uploaded to online data annotation software webKnossos (*43*). Neurites were traced in the form of skeletons. The tracings were exported as NML files and were parsed in MATLAB (release 2018a) for analyses.

Somata were manually annotated. Axon initial segments were identified based on their direction toward white matter, diameter (1 to 1.5 µm) and lack of branching; myelin ensheathment and output synapses after the end of the axon initial segment further supported the identification. The presence of a first output synapse, myelin or branching was considered the end of the axon initial segment. A total of 241 AISs were annotated in the L4 datasets and 149 in L2/3 datasets.

Apical dendrites (ADs) were identified based on their cortical direction, diameter (1 to 3 µm) and branching patterns (either no branch or only oblique branches; oblique branches of the ADs were identified by branching angles of less than 15°), and high propensity to occur in bundles. Axons innervating ADs were seeded from the shafts of clear ADs. Then, when all output synapses of the innervating axon were annotated, all postsynaptic targets were evaluated whether they also fulfilled the AD criterion. Based on calibrations in an additional dataset from L5, we estimate that most of the ADs were from L5 pyramidal cells, not L4 star pyramidal cells.

All annotations were performed by an expert annotator, and a subset of synapses and targets were proofread by another expert and the same annotator. Re-annotation of 1219 synapses and synaptic targets yielded 95.9% agreement with the initial annotation, none of the conclusions was affected by the 50 mismatches out of 1219 checked annotations.

Axon reconstruction

For a given postsynaptic target class (somata, ADs or AISs), a target was chosen at random. The synapses made onto the target were identified based on the presence of a presynaptic vesicle cloud and postsynaptic density [as described in (*44, 45, 47*), see data S1]. A skeleton node was placed in the presynaptic axon's vesicle cloud and was commented as "seed synapse" (first synapse). The axon was then skeleton-traced in the entire dataset volume. At every subsequent synapse location, a node was placed in the vesicle cloud and commented with the corresponding postsynaptic target's identity (i.e., if the postsynaptic target was soma, AD, AIS, dendritic shaft, dendritic spine, glia or somatic spines and filopodium). This was iterated for multiple seed synapses from multiple targets belonging to each target class (somata, ADs and AISs). Based

on the postsynaptic target of the first synapse, the axons were classified as soma-innervating, AD-innervating or AIS-innervating (Fig. 2, D and E, and Table 1). In rare cases, axons had a majority of their output synapses onto spines, and were therefore classified as excitatory and not included in further analysis [see (38, 45) and fig. S5 for further calibration]. For AD innervation, only synapses onto the main AD shaft were considered, not those onto oblique dendrites. For somatic synapses, those made onto somatic spines or somatic filopodia were analyzed separately [fig. S1].

Connectomes
The output synapses of the annotated axons were displayed as a connectivity matrix in which each row indicated the synapses formed by one axon on different postsynaptic targets (reported in columns, Fig. 2, D and E). The seed synapses of these axons were included in the display of connectomes. The bulk soma innervation fraction for soma-seeded axons was calculated by dividing the sum of synapses onto somata by the total number of output synapses made by these axons, with seed synapses excluded when computing these fractions (see Fig. 2, B and C, for other targets). Conditional innervation of a given target class by an axon was calculated by dividing the number of on-target synapses made by the axon by its total number of synapses (excluding the seed synapse).

Analysis of innervation multiplicity
The average number of synapses a presynaptic axon made onto an individual target (a particular soma or a particular apical dendrite, Fig. 3, F to H) was calculated by dividing the sum of synapses onto the target class (any soma, any apical dendrite) by the total number of individual targets from that target class that were innervated by the axon (including seed synapses).

Synaptic input mapping of somata
For mapping the complete set of all synaptic inputs on the cell bodies of excitatory cells, we identified all synapses made onto the somatic surface of 5 somata at each age (Fig. 3, I and J). For an analysis of synapses made on somatic spines and filopodial processes, see fig. S1.

Soma size
Soma size was determined as the equivalent diameter obtained from the surface area estimate of the soma. The surface area was determined by contouring the soma outline in all image planes using webKnossos, and fitting an isosurface to these isolines in MATLAB (R2018a). For each age group, 10 to 13 somatic diameters were determined (Fig. 3J).

Synapse densities
Axonal synapse densities were calculated by dividing the total number of output synapses from a given axon (including the seed synapse) by its total skeleton path length in the dataset (Fig. 4, B and E). The cumulative synapse density for all axons seeded from the same postsynaptic target class was calculated by dividing the total number of output synapses (made by all axons) by the sum of all axons' path lengths. On-target synapse density was calculated by dividing the total number of on-target synapses made by an axon (including the seed synapse) by its path length Bulk on-target synapse densities were computed by dividing the number of all on-target synapses of all axons by the total path length of all axons

Innervation of proximal versus distal dendrites
We classified non-somatic synapses as proximal or distal based on their location on the dendrites of the postsynaptic cell. All synapses which were made on dendritic processes emanating from the soma within 20 μm from soma and onto a 1st or 2nd order dendritic branch were considered proximal; all other synapses were classified as distal synapses (Fig. 4G). Next, we computed the axonal synapse density of proximal and distal off-target synapses, separately (Fig. 4H). In this analysis, synapses made on somatic spines and filopodial processes were included as proximal synapses. Note that proximal dendrites with a cell body adjacent to the imaged dataset were not identified, thus our identification of proximal synapses corresponds to a lower-bound estimate.

Input mapping of axon initial segments and identification of axo-axonic axons in L2/3
We identified pyramidal cells in the L2/3 datasets based on their somato-dendritic morphology and annotated the corresponding axon initial segment and its input synapses. For mapping the input synapses, each of these synapses was then considered as a seed synapse for reconstructing the presynaptic axons in the entire dataset and its other output synapses. Based on the innervation pattern of these axons, they were classified as axo-axonic or non-axo-axonic using hierarchical clustering (only axons with at least 7 synapses were classified; function clusterdata in Matlab, Ward's method, Euclidean distance, 2 clusters) on axonal synapse density and fraction of synapses onto axon initial segments per axon (Fig. 5D).

Axo-axonic cartridge analysis
An axon cartridge was defined as the stretch of an axon which was adjacent to an axon initial segment and made at least 3 synapses on the same axon initial segment (Fig. 6, E and H). We quantified the on-target synapse density of these cartridges by dividing the number of synapses onto axon initial segments from that cartridge by its path length (Fig. 6E).

Axonal path length density

We measured the addition of axonal cartridges in axo-axonic axons at P28 by separating axonal paths that had at least 3 synapses onto the same AIS and maximally one off-target synapse. Then, those axonal paths that fulfilled these criteria and had an axonal ending were identified; in addition those axonal stretches that fulfilled these criteria but were "en-passant", i.e., without an axonal ending were also identified. This yielded a minimal (only cartridges with an axonal ending) and maximal (including cartridges "en-passant") cartridge path length at P28; cartridge addition model predictions were computed for both values and are reported as ranges (see next section).

Cartridge addition model

We tested a simple model that the increase of target-preference in axo-axonic axons between P14 and P28 can be fully explained by the addition of axonal cartridges that establish exclusively synapses onto axon initial segments. Then, the predicted fractional target preference at P28 is given as

$$Frac^{AIS}_{P28} = \frac{\left(n_{syn,P14}{}^{\rightarrow AIS} \big/ L_{P14} + \Delta L^* d_{syn}{}^{Cart} \right)}{\left(n_{syn,P14}{}^{\rightarrow \varnothing} \big/ L_{P14} + n_{syn,P14}{}^{\rightarrow AIS} \big/ L_{P14} + \Delta L^* d_{syn}{}^{Cart} \right)}$$

with $n_{syn,P14}{}^{\rightarrow AIS} \big/ L_{P14}$ the length density of synapses onto axon initial segments at P14 (see Table 1) and $n_{syn,P14}{}^{\rightarrow \varnothing} \big/ L_{P14}$ the density of synapses onto other targets at P14 per micrometer axo-axonic axon path length; ΔL the relative cartridge length per axon length at P28: $\Delta L = L_{cart}/L_{non-cart}$ with $L_{cart}/L_{non-cart}$ measured as described in the previous section; and $d_{syn}{}^{Cart}$ the density of AIS output synapses per axonal cartridge length at P28 (see Fig. 6E and Table 1).

For integrating additional antispecific pruning, we replaced $n_{syn,P14}{}^{\rightarrow \varnothing}$ in above formula by $\left(1 - f_{prun}\right)^* n_{syn,P14}{}^{\rightarrow \varnothing}$ with f_{prun} the fraction of off-target synapses pruned between P14 and P28. Then, we determined f_{prun} such that $Frac^{AIS}{}_{P28}$ equals the measured fractional AIS preference of axo-axonic axons at P28.

Statistics

All statistical tests were performed using MATLAB and the Statistics Toolbox (Releases 2013, 2017, 2018b, 2020, The MathWorks, Inc.) and are reported in Table 1. For fractional innervation and synapse densities, bulk averages over all reconstructed axons were computed. The variability of the average was determined by bootstrap (1000 repetitions, sampling by replacement) yielding an estimate of the standard error. Sample comparisons were done by bootstrapping each distribution and determining the fraction of cases in which the bootstrapped mean of one sample was smaller (or larger) than the other (10^6 bootstrap comparisons for each

pair of datasets). For all other tests, between-group comparisons were done using two-sample Kolmogorov-Smirnov test (*kstest2*) for probabilities or fractions and Wilcoxon rank sum test otherwise.

Analysis code is available on GitLab (*59*).

Data availability

All 3D-EM data, reconstructions and synapse annotations will be made publicly available upon publication at webknossos.org. For review, the datasets can be browsed via the following links.

L4 datasets

1.) P5: https://webknossos.brain.mpg.de/annotations/Explorational/5f097b27010000790041907c?token=PHmjUiqI-wSF5j_3m3NewxA#3377,3798,1731,0,51.095,24

2.) P7 (d1): https://webknossos.brain.mpg.de/annotations/Explorational/5f097d9e010000684f419095?token=yLaZU9zIOpWAYpM5hIZKRw#3827,4657,2562,0,46.451,13851

3.) P7 (d2, control): https://webknossos.brain.mpg.de/annotations/Explorational/5f097ea2010000d05041909c?token=j1OMURYgwITqSpMFq3Pj-w#3286,3914,1057,0,34.897,2446

4.) P9 (d1): https://webknossos.brain.mpg.de/annotations/Explorational/5f098052010000644f4190ae?token=gMxrKSnIXkUW-lFZ1H9IQg#3471,3841,1499,0,31.160,16827

5.) P9 (d2): https://webknossos.brain.mpg.de/annotations/Explorational/5f0982bb0100007a004190e7#4999,4207,1207,0,31.857,4709

6.) P9 (d3, control): https://webknossos.brain.mpg.de/annotations/Explorational/5f09834c01000079004190f3#3561,3978,1222,0,31.716,2069

7.) P14 (d1): https://webknossos.brain.mpg.de/annotations/Explorational/5f098547010000644f41910b#2961,2596,2396,0,38.806,31

8.) P14 (d2): https://webknossos.brain.mpg.de/annotations/Explorational/5f0986e70100007a0041912f#2706,5196,1768,0,35.682,28717

9.) P28: https://webknossos.brain.mpg.de/annotations/Explorational/5f098a230100000f00419189#2547,4286,1960,0,33.854,23869

L2/3 datasets

1.) P9: https://webknossos.brain.mpg.de/annotations/Explorational/5f098af00100000f0041919d#4590,6017,2004,0,59.174,20184

2.) P14: https://webknossos.brain.mpg.de/annotations/Explorational/5f098d370100004e244191d1#6158,4347,2042,0,41.566,17586

3.) P28: https://webknossos.brain.mpg.de/annotations/Explorational/5f098e390100007a004191ed#4157,3279,3551,0,66.757,24650

4.) P56 (PPC, control): https://webknossos.brain.mpg.de/annotations/Explorational/5f0996160100000f004192db?token=mJbnSmb9YsBHfn8J0mEhKQ#5770,2523,2313,0,46.431,166

Control reannotations by expert consensus

1.) P5: https://webknossos.brain.mpg.de/annotations/Explorational/5f5923680100007400c81ff4?token=PHmjUiqIwSF5j_3m3NewxA#3640,4052,1012,0,21.664,2550

2.) P7-d1: https://webknossos.brain.mpg.de/annotations/Explorational/5f4c8b71010000b3b13f9873?token=8NxQBXju36abb1Uhl9XuZw#3371,4434,2656,0,26.205,37966

3.) P7-d2: https://webknossos.brain.mpg.de/annotations/Explorational/5f50a4110100000e00d34ce5?token=j1OMURYgwITqSpMFq3Pj-w#3202,4045,1303,0,21.670,19465

4.) P9-d1: https://webknossos.brain.mpg.de/annotations/Explorational/5f3d78560100006c001af494?token=gMxrKSnIXkUW-lFZ1H9IQg#3572,4078,1605,0,19.343,43555

5.) P9-d3: https://webknossos.brain.mpg.de/annotations/Explorational/5f50bc2d01000078002a307a?token=P8ApNtJzXur2tYlPLcr7Jg#2893,3743,1064,0,19.194,13817

REFERENCES AND NOTES

1. P. Rakic, J. P. Bourgeois, M. F. Eckenhoff, N. Zecevic, P. S. Goldman-Rakic, Concurrent overproduction of synapses in diverse regions of the primate cerebral cortex. *Science* **232**, 232–235 (1986). doi:10.1126/science.3952506 Medline
2. S. Ramón y Cajal, *Histology of the Nervous System* (Oxford Univ. Press, 1995).
3. J. De Felipe, P. Marco, A. Fairén, E. G. Jones, Inhibitory synaptogenesis in mouse somatosensory cortex. *Cereb. Cortex* **7**, 619–634 (1997). doi:10.1093/cercor/7.7.619 Medline
4. K. D. Micheva, C. Beaulieu, Quantitative aspects of synaptogenesis in the rat barrel field cortex with special reference to GABA circuitry. *J. Comp. Neurol.* **373**, 340–354 (1996). doi:10.1002/(SICI)1096-9861(19960923)373:3<340:AID-CNE3>3.0.CO;2-2 Medline
5. J. P. Bourgeois, P. Rakic, Changes of synaptic density in the primary visual cortex of the macaque monkey from fetal to adult stage. *J. Neurosci.* **13**, 2801–2820 (1993). doi:10.1523/JNEUROSCI.13-07-02801.1993 Medline
6. T. C. Südhof, Towards an understanding of synapse formation. *Neuron* **100**, 276–293 (2018). doi:10.1016/j.neuron.2018.09.040 Medline
7. J. R. Sanes, S. L. Zipursky, Synaptic specificity, recognition molecules, and assembly of neural circuits. *Cell* **181**, 536–556 (2020). doi:10.1016/j.cell.2020.04.008 Medline
8. E. Favuzzi, R. Deogracias, A. Marques-Smith, P. Maeso, J. Jezequel, D. Exposito-Alonso, M. Balia, T. Kroon, A. J. Hinojosa, E. F Maraver, B. Rico, Distinct molecular programs regulate synapse specificity in cortical inhibitory circuits. *Science* **363**, 413–417 (2019). doi:10.1126/science.aau8977 Medline
9. C. Mayer, C. Hafemeister, R. C. Bandler, R. Machold, R. Batista Brito, X. Jaglin, K. Allaway, A. Butler, G. Fishell, R. Satija, Developmental diversification of cortical inhibitory interneurons. *Nature* **555**, 457–462 (2018). doi:10.1038/nature25999 Medline
10. Z. J. Huang, G. Di Cristo, F. Ango, Development of GABA innervation in the cerebral and cerebellar cortices. *Nat. Rev. Neurosci.* **8**, 673–686 (2007). doi:10.1038/nrn2188 Medline
11. D. G. Southwell, M. F. Paredes, R. P. Galvao, D. L. Jones, R. C. Froemke, J. Y. Sebe, C. Alfaro-Cervello, Y. Tang, J. M. Garcia-Verdugo, J. L. Rubenstein, S. C. Baraban, A. Alvarez-Buylla, Intrinsically determined cell death of developing cortical interneurons. *Nature* **491**, 109–113 (2012). doi:10.1038/nature11523 Medline
12. Y. Kubota, F. Karube, M. Nomura, Y. Kawaguchi, The diversity of cortical inhibitory synapses. *Front. Neural Circuits* **10**, 27 (2016). doi:10.3389/fncir.2016.00027 Medline
13. G. A. Ascoli, L. Alonso-Nanclares, S. A. Anderson, G. Barrionuevo, R. Benavides-Piccione, A. Burkhalter, G. Buzsáki, B. Cauli, J. Defelipe, A. Fairén, D. Feldmeyer, G. Fishell, Y. Fregnac, T. F. Freund, D. Gardner, E. P. Gardner, J. H. Goldberg, M. Helmstaedter, S. Hestrin, F. Karube, Z. F. Kisvárday, B. Lambolez, D. A. Lewis, O. Marin, H. Markram, A. Muñoz, A. Packer, C. C. Petersen, K. S. Rockland, J. Rossier, B. Rudy, P. Somogyi, J. F. Staiger, G. Tamas, A. M. Thomson, M. Toledo-Rodriguez, Y. Wang, D. C. West, R. Yuste; Petilla Interneuron Nomenclature Group, Petilla terminology: Nomenclature of features of GABAergic interneurons of the cerebral cortex. *Nat. Rev. Neurosci.* **9**, 557–568 (2008). doi:10.1038/nrn2402 Medline
14. R. Yuste, M. Hawrylycz, N. Aalling, A. Aguilar-Valles, D. Arendt, R. A. Arnedillo, G. A. Ascoli, C. Bielza, V. Bokharaie, T. B. Bergmann, I. Bystron, M. Capogna, Y. Chang, A. Clemens, C. P. J. de Kock, J. DeFelipe, S. E. Dos Santos, K. Dunville, D. Feldmeyer, R. Fiáth, G. J. Fishell, A. Foggetti, X. Gao, P. Ghaderi, N. A. Goriounova, O. Güntürkün, K. Hagihara, V. J. Hall, M. Helmstaedter, S. Herculano, M. M. Hilscher, H. Hirase, J. Hjerling-Leffler, R. Hodge, J. Huang, R. Huda, R. Khodosevich, O. Kiehn, H. Koch, E. S. Kuebler, M. Kühnemund, P. Larrañaga, B. Lelieveldt, E. L. Louth, J. H. Lui, H. D. Mansvelder, O. Marin, J. Martinez-Trujillo, H. Moradi Chameh, A. Nath, M. Nedergaard, P. Němec, N. Ofer, U. G. Pfisterer, S. Pontes, W. Redmond, J. Rossier, J. R. Sanes, R. Scheuermann, E. Serrano-Saiz, J. F. Steiger, P. Somogyi, G. Tamás, A. S. Tolias, M. A. Tosches, M. T. García, H. M. Vieira, C. Wozny, T. V. Wuttke, L. Yong, J. Yuan, H. Zeng, E. Lein, A community-based transcriptomics classification and nomenclature of neocortical cell types. *Nat. Neurosci.* **23**, 1456–1468 (2020). doi:10.1038/s41593-020-0685-8 Medline
15. Y. Gonchar, A. Burkhalter, Three distinct families of GABAergic neurons in rat visual cortex. *Cereb. Cortex* **7**, 347–358 (1997). doi:10.1093/cercor/7.4.347 Medline
16. B. Cauli, E. Audinat, B. Lambolez, M. C. Angulo, N. Ropert, K. Tsuzuki, S. Hestrin, J. Rossier, Molecular and physiological diversity of cortical nonpyramidal cells. *J. Neurosci.* **17**, 3894–3906 (1997). doi:10.1523/JNEUROSCI.17-10-03894.1997 Medline
17. Y. Kawaguchi, Y. Kubota, GABAergic cell subtypes and their synaptic connections in rat frontal cortex. *Cereb. Cortex* **7**, 476–486 (1997). doi:10.1093/cercor/7.6.476 Medline
18. P. Somogyi, A specific 'axo-axonal' interneuron in the visual cortex of the rat. *Brain Res.* **136**, 345–350 (1977). doi:10.1016/0006-8993(77)90808-3 Medline
19. G. Miyoshi, S. J. Butt, H. Takebayashi, G. Fishell, Physiologically distinct temporal cohorts of cortical interneurons arise from telencephalic Olig2-expressing precursors. *J. Neurosci.* **27**, 7786–7798 (2007). doi:10.1523/JNEUROSCI.1807-07.2007 Medline
20. G. Miyoshi, G. Fishell, GABAergic interneuron lineages selectively sort into specific cortical layers during early postnatal development. *Cereb. Cortex* **21**, 845–852 (2011). doi:10.1093/cercor/bhq155 Medline

21. F. Karube, Y. Kubota, Y. Kawaguchi, Axon branching and synaptic bouton phenotypes in GABAergic nonpyramidal cell subtypes. *J. Neurosci.* **24**, 2853–2865 (2004). doi:10.1523/JNEUROSCI.4814-03.2004 Medline

22. G. Di Cristo, C. Wu, B. Chattopadhyaya, F. Ango, G. Knott, E. Welker, K. Svoboda, Z. J. Huang, Subcellular domain-restricted GABAergic innervation in primary visual cortex in the absence of sensory and thalamic inputs. *Nat. Neurosci.* **7**, 1184–1186 (2004). doi:10.1038/nn1334 Medline

23. B. Chattopadhyaya, G. Di Cristo, H. Higashiyama, G. W. Knott, S. J. Kuhlman, E. Welker, Z. J. Huang, Experience and activity-dependent maturation of perisomatic GABAergic innervation in primary visual cortex during a postnatal critical period. *J. Neurosci.* **24**, 9598–9611 (2004). doi:10.1523/JNEUROSCI.1851-04.2004 Medline

24. S. Bähr, J. R. Wolff, Postnatal development of axosomatic synapses in the rat visual cortex: Morphogenesis and quantitative evaluation. *J. Comp. Neurol.* **233**, 405–420 (1985). doi:10.1002/cne.902330309 Medline

25. P. Somogyi, Z. F. Kisvárday, K. A. Martin, D. Whitteridge, Synaptic connections of morphologically identified and physiologically characterized large basket cells in the striate cortex of cat. *Neuroscience* **10**, 261–294 (1983). doi:10.1016/0306-4522(83)90133-1 Medline

26. M. I. Daw, M. C. Ashby, J. T. Isaac, Coordinated developmental recruitment of latent fast spiking interneurons in layer IV barrel cortex. *Nat. Neurosci.* **10**, 453–461 (2007). doi:10.1038/nn1866 Medline

27. S. Pangratz-Fuehrer, S. Hestrin, Synaptogenesis of electrical and GABAergic synapses of fast-spiking inhibitory neurons in the neocortex. *J. Neurosci.* **31**, 10767–10775 (2011). doi:10.1523/JNEUROSCI.6655-10.2011 Medline

28. L. Lim, J. M. P. Pakan, M. M. Selten, A. Marques-Smith, A. Llorca, S. E. Bae, N. L. Rochefort, O. Marín, Optimization of interneuron function by direct coupling of cell migration and axonal targeting. *Nat. Neurosci.* **21**, 920–931 (2018). doi:10.1038/s41593-018-0162-9 Medline

29. E. G. Jones, Varieties and distribution of non-pyramidal cells in the somatic sensory cortex of the squirrel monkey. *J. Comp. Neurol.* **160**, 205–267 (1975). doi:10.1002/cne.901600204 Medline

30. J. Szentágothai, The 'module-concept' in cerebral cortex architecture. *Brain Res.* **95**, 475–496 (1975). doi:10.1016/0006-8993(75)90122-5 Medline

31. Y. Gonchar, S. Turney, J. L. Price, A. Burkhalter, Axo-axonic synapses formed by somatostatin-expressing GABAergic neurons in rat and monkey visual cortex. *J. Comp. Neurol.* **443**, 1–14 (2002). doi:10.1002/cne.1425 Medline

32. A. R. Woodruff, S. A. Anderson, R. Yuste, The enigmatic function of chandelier cells. *Front. Neurosci.* **4**, 201 (2010). doi:10.3389/fnins.2010.00201 Medline

33. Y. Tai, N. B. Gallo, M. Wang, J. R. Yu, L. Van Aelst, Axo-axonic innervation of neocortical pyramidal neurons by GABAergic chandelier cells requires ankyrinG-associated L1CAM. *Neuron* **102**, 358–372.e9 (2019). doi:10.1016/j.neuron.2019.02.009 Medline

34. Y. Tai, J. A. Janas, C. L. Wang, L. Van Aelst, Regulation of chandelier cell cartridge and bouton development via DOCK7-mediated ErbB4 activation. *Cell Rep.* **6**, 254–263 (2014). doi:10.1016/j.celrep.2013.12.034 Medline

35. H. Taniguchi, J. Lu, Z. J. Huang, The spatial and temporal origin of chandelier cells in mouse neocortex. *Science* **339**, 70–74 (2013). doi:10.1126/science.1227622 Medline

36. M. Inan, L. Blázquez-Llorca, A. Merchán-Pérez, S. A. Anderson, J. DeFelipe, R. Yuste, Dense and overlapping innervation of pyramidal neurons by chandelier cells. *J. Neurosci.* **33**, 1907–1914 (2013). doi:10.1523/JNEUROSCI.4049-12.2013 Medline

37. A. Pan-Vazquez, W. Wefelmeyer, V. Gonzalez Sabater, G. Neves, J. Burrone, Activity-dependent plasticity of axo-axonic synapses at the axon initial segment. *Neuron* **106**, 265–276.e6 (2020). doi:10.1016/j.neuron.2020.01.037 Medline

38. A. Motta, M. Berning, K. M. Boergens, B. Staffler, M. Beining, S. Loomba, P. Hennig, H. Wissler, M. Helmstaedter, Dense connectomic reconstruction in layer 4 of the somatosensory cortex. *Science* **366**, eaay3134 (2019). doi:10.1126/science.aay3134 Medline

39. X. Wu, Y. Fu, G. Knott, J. Lu, G. Di Cristo, Z. J. Huang, GABA signaling promotes synapse elimination and axon pruning in developing cortical inhibitory interneurons. *J. Neurosci.* **32**, 331–343 (2012). doi:10.1523/JNEUROSCI.3189-11.2012 Medline

40. A. M. Wilson, R. Schalek, A. Suissa-Peleg, T. R. Jones, S. Knowles-Barley, H. Pfister, J. W. Lichtman, Developmental rewiring between cerebellar climbing fibers and Purkinje cells begins with positive feedback synapse addition. *Cell Rep.* **29**, 2849–2861.e6 (2019). doi:10.1016/j.celrep.2019.10.081 Medline

41. D. P. Schafer, E. K. Lehrman, A. G. Kautzman, R. Koyama, A. R. Mardinly, R. Yamasaki, R. M. Ransohoff, M. E. Greenberg, B. A. Barres, B. Stevens, Microglia sculpt postnatal neural circuits in an activity and complement-dependent manner. *Neuron* **74**, 691–705 (2012). doi:10.1016/j.neuron.2012.03.026 Medline

42. W. Denk, H. Horstmann, Serial block-face scanning electron microscopy to reconstruct three-dimensional tissue nanostructure. *PLOS Biol.* **2**, e329 (2004). doi:10.1371/journal.pbio.0020329 Medline

43. K. M. Boergens, M. Berning, T. Bocklisch, D. Bräunlein, F. Drawitsch, J. Frohnhofen, T. Herold, P. Otto, N. Rzepka, T. Werkmeister, D. Werner, G. Wiese, H. Wissler, M. Helmstaedter, webKnossos: Efficient online 3D data annotation for connectomics. *Nat. Methods* **14**, 691–694 (2017). doi:10.1038/nmeth.4331 Medline

44. H. Schmidt, A. Gour, J. Straehle, K. M. Boergens, M. Brecht, M. Helmstaedter, Axonal synapse sorting in medial entorhinal cortex. *Nature* **549**, 469–475 (2017). doi:10.1038/nature24005 Medline

45. A. Karimi, J. Odenthal, F. Drawitsch, K. M. Boergens, M. Helmstaedter, Cell-type specific innervation of cortical pyramidal cells at their apical dendrites. *eLife* **9**, e46876 (2020). doi:10.7554/eLife.46876 Medline

46. Y. Hua, P. Laserstein, M. Helmstaedter, Large-volume en-bloc staining for electron microscopy-based connectomics. *Nat. Commun.* **6**, 7923 (2015). doi:10.1038/ncomms8923 Medline

47. B. Staffler, M. Berning, K. M. Boergens, A. Gour, P. V. Smagt, M. Helmstaedter, SynEM, automated synapse detection for connectomics. *eLife* **6**, e26414 (2017). doi:10.7554/eLife.26414 Medline

48. L. de Vivo, M. Bellesi, W. Marshall, E. A. Bushong, M. H. Ellisman, G. Tononi, C. Cirelli, Ultrastructural evidence for synaptic scaling across the wake/sleep cycle. *Science* **355**, 507–510 (2017). doi:10.1126/science.aah5982 Medline

49. S. N. Tuncdemir, B. Wamsley, F. J. Stam, F. Osakada, M. Goulding, E. M. Callaway, B. Rudy, G. Fishell, Early somatostatin interneuron connectivity mediates the maturation of deep layer cortical circuits. *Neuron* **89**, 521–535 (2016). doi:10.1016/j.neuron.2015.11.020 Medline

50. O. Marín, Developmental timing and critical windows for the treatment of psychiatric disorders. *Nat. Med.* **22**, 1229–1238 (2016). doi:10.1038/nm.4225 Medline

51. A. Ribic, M. C. Crair, T. Biederer, Synapse-selective control of cortical maturation and plasticity by parvalbumin-autonomous action of SynCAM 1. *Cell Rep.* **26**, 381–393.e6 (2019). doi:10.1016/j.celrep.2018.12.069 Medline

52. Y. Kawaguchi, Y. Kubota, Correlation of physiological subgroupings of nonpyramidal cells with parvalbumin- and calbindinD28k-immunoreactive neurons in layer V of rat frontal cortex. *J. Neurophysiol.* **70**, 387–396 (1993). doi:10.1152/jn.1993.70.1.387 Medline

53. Y. Kawaguchi, Physiological subgroups of nonpyramidal cells with specific morphological characteristics in layer II/III of rat frontal cortex. *J. Neurosci.* **15**, 2638–2655 (1995). doi:10.1523/JNEUROSCI.15-04-02638.1995 Medline

54. B. Wamsley, L. A. Ibrahim, N. Yusuf, E. Fisher, X. H. Jaglin, Q. Xu, L. Guo, A. Khodadadi-Jamayran, E. Favuzzi, Y. Yuan, J. Dimidschstein, R. Darnell, G. Fishell, Nova proteins direct synaptic integration of somatostatin interneurons through activity-dependent alternative splicing. bioRxiv 845230 [Preprint]. 16 November 2019. https://doi.org/10.1101/845230.

55. A. Steinecke, E. Hozhabri, S. Tapanes, Y. Ishino, H. Zeng, N. Kamasawa, H. Taniguchi, Neocortical chandelier cells developmentally shape axonal arbors through reorganization but establish subcellular synapse specificity without refinement. *eNeuro* **4**, ENEURO.0057-17.2017 (2017). doi:10.1523/ENEURO.0057-17.2017 Medline

56. T. F. Freund, I. Katona, Perisomatic inhibition. *Neuron* **56**, 33–42 (2007). doi:10.1016/j.neuron.2007.09.012 Medline

57. P. D. Whissell, J. D. Cajanding, N. Fogel, J. C. Kim, Comparative density of CCK- and PV-GABA cells within the cortex and hippocampus. *Front. Neuroanat.* **9**, 124 (2015). doi:10.3389/fnana.2015.00124 Medline

58. J. Lu, J. Tucciarone, N. Padilla-Coreano, M. He, J. A. Gordon, Z. J. Huang, Selective inhibitory control of pyramidal neuron ensembles and cortical subnetworks by chandelier cells. *Nat. Neurosci.* **20**, 1377–1383 (2017). doi:10.1038/nn.4624 Medline

59. developmentalConnectomics, project ID 4598, MPCDF GitLab (2020); https://doi.org/10.17617/1.br202001.
60. A. Dufour, A. Rollenhagen, K. Sätzler, J. H. R. Lübke, Development of synaptic boutons in layer 4 of the barrel field of the rat somatosensory cortex: A quantitative analysis. *Cereb. Cortex* **26**, 838–854 (2016). Medline
61. J. C. Fiala, M. Feinberg, V. Popov, K. M. Harris, Synaptogenesis via dendritic filopodia in developing hippocampal area CA1. *J. Neurosci.* **18**, 8900–8911 (1998). doi:10.1523/JNEUROSCI.18-21-08900.1998 Medline
62. K. M. Harris, F. E. Jensen, B. Tsao, Three-dimensional structure of dendritic spines and synapses in rat hippocampus (CA1) at postnatal day 15 and adult ages: Implications for the maturation of synaptic physiology and long-term potentiation. *J. Neurosci.* **12**, 2685–2705 (1992). doi:10.1523/JNEUROSCI.12-07-02685.1992 Medline
63. K. E. Sorra, J. C. Fiala, K. M. Harris, Critical assessment of the involvement of perforations, spinules, and spine branching in hippocampal synapse formation. *J. Comp. Neurol.* **398**, 225–240 (1998). doi:10.1002/(SICI)1096-9861(19980824)398:2<225:AID-CNE5>3.0.CO:2-2 Medline
64. A. E. El-Husseini, E. Schnell, D. M. Chetkovich, R. A. Nicoll, D. S. Bredt, PSD-95 involvement in maturation of excitatory synapses. *Science* **290**, 1364–1368 (2000). Medline
65. M. Sheng, E. Kim, The postsynaptic organization of synapses. *Cold Spring Harbor Perspect. Biol.* **3**, a005678 (2011). doi:10.1101/cshperspect.a005678 Medline
66. J. E. Vaughn, Fine structure of synaptogenesis in the vertebrate central nervous system. *Synapse* **3**, 255–285 (1989). doi:10.1002/syn.890030312 Medline
67. S. Preibisch, S. Saalfeld, P. Tomancak, Globally optimal stitching of tiled 3D microscopic image acquisitions. *Bioinformatics* **25**, 1463–1465 (2009). doi:10.1093/bioinformatics/btp184 Medline

SUPPLEMENTARY MATERIALS

Table 1. Quantification of postnatal inhibitory circuit development in L4 and L2/3. Bootstrapped means and standard errors of means and probabilities from bootstrapped comparison reported unless otherwise indicated, see methods. n_{sy}, number of synapses; n_{ax}, number of axons. Innervation multiplicity: Number of synapses per axon and individual target. AIS: axon initial segment. L_{ax}: axonal path length. 2-S. t test: two-sample Student's t test. rs: Wilcoxon rank-sum test. Note that to account for the number of initial comparisons, only P values below 10^{-3} were considered; all reported effects had substantially lower P values in the initial comparisons.

|	P7	P9	P14	P28
Conditional reinnervation				
p(soma|soma)	$6.01 \pm 1.07\%^{*}$, $n_{sy} = 1119$, $n_{ax} = 21$	$16.07 \pm 1.46\%^{*}$, $n_{sy} = 1110$, $n_{ax} = 52$	$23.38 \pm 1.76\%$, $n_{sy} = 1440$, $n_{ax} = 67$	$17.45 \pm 2.05\%$, $n_{sy} = 1143$, $n_{ax} = 20$
		$P = 10^{-6}$	$P = 1.6 \times 10^{-4}$	$P = 0.019$
p(AD|AD)	$14.62 \pm 4.12\%$, $n_{sy} = 232$, $n_{ax} = 20$	$15.88 \pm 3.02\%$, $n_{sy} = 462$, $n_{ax}=59$	$25.16 \pm 2.94\%$, $n_{sy} = 1241$, $n_{ax} = 116$	$23.28 \pm 4.50\%$, $n_{sy} = 371$, $n_{ax} = 23$
		$P = 0.59$	$P = 0.014$	$P = 0.61$
Innervation multiplicity[†,‡]				
Onto soma	1.16 ± 0.06	1.39 ± 0.06	1.83 ± 0.08	2.20 ± 0.13
		$P = 0.19$ (rs)	$P = 3.5 \times 10^{-4}$ (rs)	$P = 0.026$ (rs)
Onto AD	1.41 ± 0.18	1.40 ± 0.08	1.99 ± 0.14	2.08 ± 0.26
		$P = 0.99$ (rs)	$P = 0.0016$ (rs)	$P = 0.47$ (rs)
Total number of input synapses per soma[‡]	5.2 ± 0.97, $n_{som} = 5$	8 ± 0.45, $n_{som} = 5$	47 ± 2.02, $n_{som} = 5$	75.2 ± 3.20, $n_{som} = 5$
		$P = 0.04$ (rs)	$P = 0.008$ (rs)	$P = 0.008$ (rs)
Synapse density along axons (per micrometer path length)				
Soma-seeded axons				
All synapses	0.168 ± 0.014, $n_{sy} = 1119$, $n_{ax} = 21$	0.088 ± 0.009, $n_{sy} = 1110$, $n_{ax} = 52$	0.132 ± 0.007, $n_{sy} = 1437$, $n_{ax} = 67$	0.248 ± 0.014, $n_{sy} = 1143$, $n_{ax} = 20$
		$P = 10^{-6}$	$P = 3.6 \times 10^{-5}$	$P = 10^{-6}$
Synapses onto proximal dendrites	0.023 ± 0.004, $n_{sy} = 1119$	0.017 ± 0.003, $n_{sy} = 1110$		
		$P = 0.12$, 2-S. t test		
Synapses onto distal dendrites	0.132 ± 0.012	0.053 ± 0.01		
		$P = 7.8 \times 10^{-6}$, 2-S. t test		

Apical dendrite-seeded axons				
All synapses	0.099 ± 0.013, $n_{sy} = 232$, $n_{ax} = 20$	0.075 ± 0.006, $n_{sy} = 463$, $n_{ax} = 59$	0.11 ± 0.006, $n_{sy} = 1241$, $n_{ax} = 116$	0.184 ± 0.012, $n_{sy} = 371$, $n_{ax} = 23$
		$P = 0.031$	$P = 2 \times 10^{-6}$	$P = 10^{-6}$
AIS input synapses in L2/3				
Made by axo-axonic axons§	None	0%	$32.8 \pm 6.1\%$, $n = 8$ AIS, $n_{sy} = 16$ of 61	$60.9 \pm 4.9\%$, $n = 5$ AIS, $n_{sy} = 87$ of 146
			$P = 0.016$¶	
Conditional reinnervation p(AIS|AIS)‡				
By axo-axonic axons			$56.98 \pm 4.98\%$, $n_{ax} = 5$	$89.36 \pm 2.09\%$, $n_{ax} = 10$
			$P = 6.4 \times 10^{-4}$¶	
By non-axo-axonic axons		$6.52 \pm 2.98\%$, $n_{ax} = 7$	$2.42 \pm 0.76\%$, $n_{ax} = 49$	$2.13 \pm 0.64\%$, $n_{ax} = 41$
			$P > 0.9$¶	
Synapse density along axons (per micrometer path length)‡				
Axo-axonic axons			0.042 ± 0.002, $L_{ax} = 2.19$ mm	0.052 ± 0.008, $L_{ax} = 6.52$ mm
			$P = 0.09$ (rs)	
Non-axo-axonic axons		0.043 ± 0.014, $L_{ax} = 2.31$ mm	0.102 ± 0.009, $L_{ax} = 8.98$ mm	0.179 ± 0.009, $L_{ax} = 7.31$ mm
			$P = 4.7 \times 10^{-11}$ (rs)	
Synapse density along axo-axonic cartridges (per micrometer)				0.24 ± 0.013
Relative cartridge length (micrometer cartridge per micrometer axonal trunk)				0.16–0.24#

*When including synaptic filopodia as targets, reinnervation fraction increases to $7.74 \pm 2.64\%$ at P7 ($n = 106$ synapses) and $21.27 \pm 2.94\%$ at P9 ($n = 277$ synapses), i.e., a 2.75-fold increase between P7 and P9, $P = 0.01$.　†Same number of axons analyzed as for conditional innervation.　‡Bulk average ± sample SEM.　§Fractions from identified non-axo-axonic axons: 50%, 37% at P14, P28; difference from 100%: axons with less than 7 synapses.　¶Two-sample Kolmogorov-Smirnov test.　#Range indicates cartridges with mandatory axonal ending (lower) and with inclusion of en-passant cartridge configurations (upper), see methods.
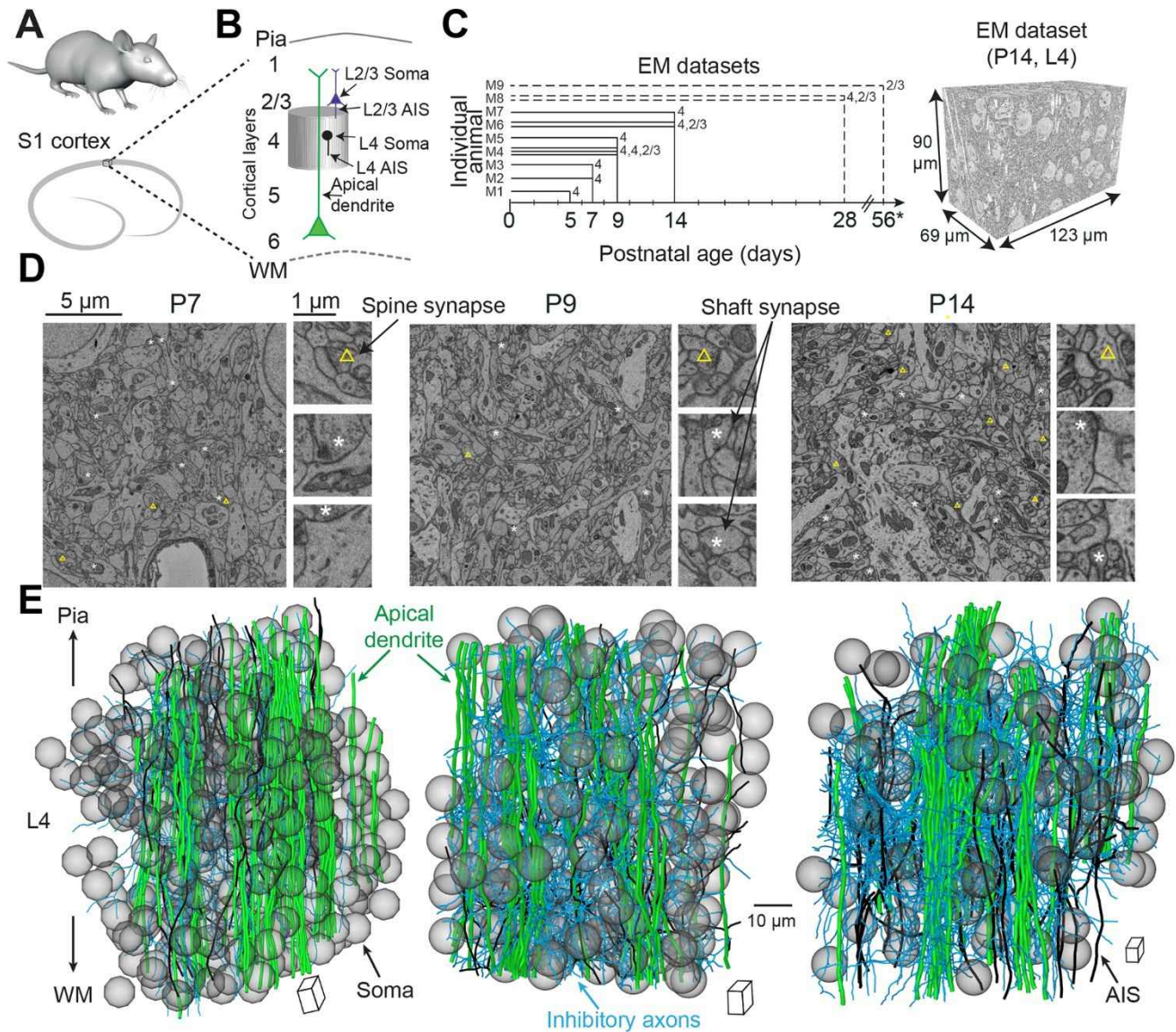
Fig. 1. Connectomic analysis in mouse primary somatosensory cortex across postnatal development.
(A and B) Sketch of mouse primary somatosensory cortex (S1) and the neuronal structures expected in 3D electron microscopy (3D-EM) datasets in cortical layers 4 and 2/3. (C) Thirteen 3D-EM datasets acquired from the cortex of nine mice (M1 to M9) at 5, 7, 9, 14, 28 and 56 postnatal days (P) of age [P28 and P56 datasets published before (*38*, *45*), dashed lines]. Example dataset shown on right. Numbers at lines indicate layer position of datasets. Datasets from M1, M3, M5, M9 were analyzed as post-hoc controls of biological variability and age. *: note that the control P56 dataset was from L2/3 of mouse posterior parietal cortex. (D) Electron micrographs from P7, P9 and P14 datasets. Examples of spine (triangle) and shaft (asterisk) synapses shown. (E) Reconstructions of presynaptic axons (blue), postsynaptic somata (gray), axon initial segments (AIS, black) and apical dendrites (green) in the P7, P9 and P14 datasets [see (C), (D), and tables S1 and S2]. WM: white matter. Sketch cubes indicated dataset orientation relative to cortical axis.
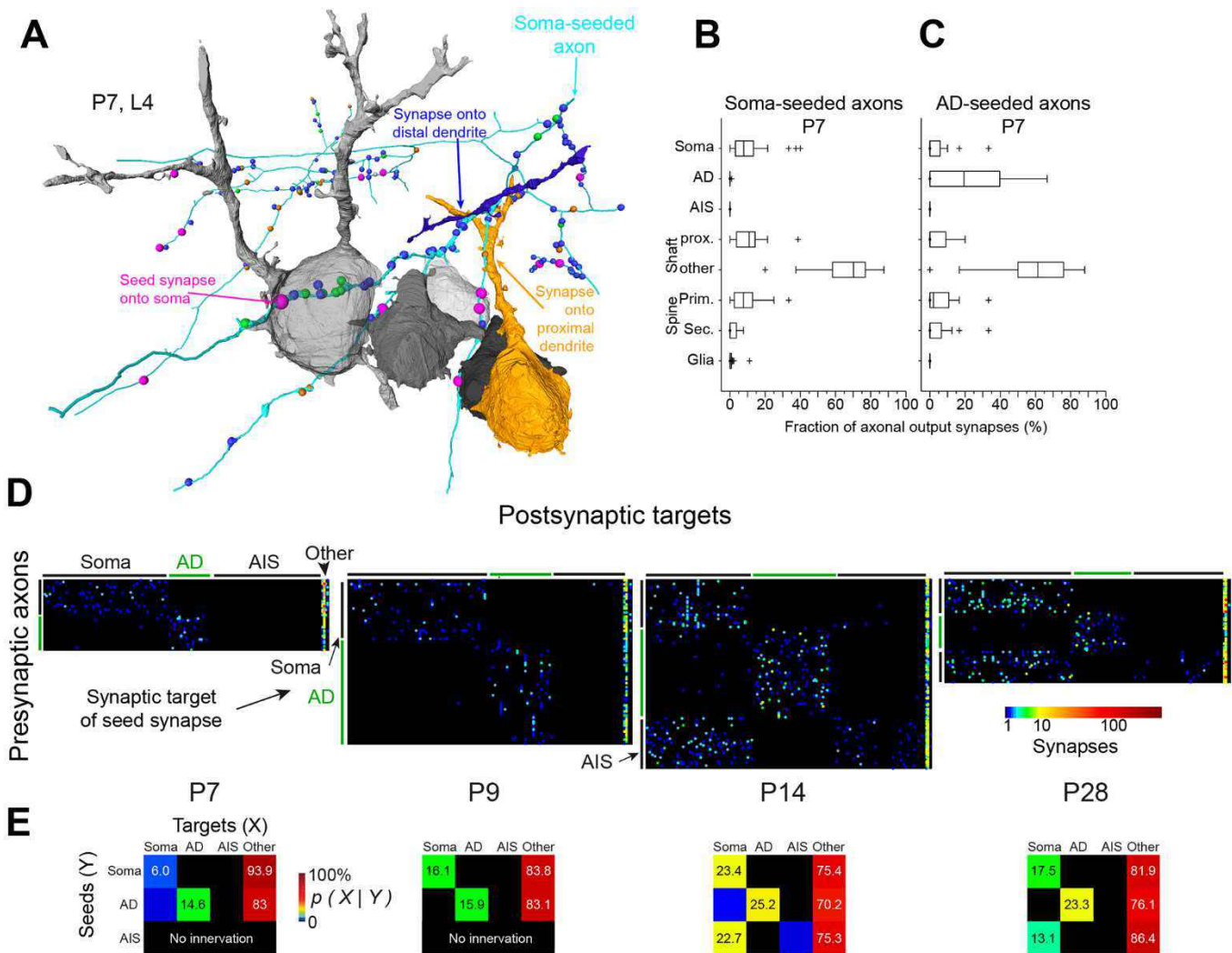
Fig. 2. Development of inhibitory connectomes. (A) Example reconstruction of a P7 soma-seeded axon (cyan), all of its output synapses (spheres, *n* = 167), and all their postsynaptic targets (soma, magenta; proximal dendritic shaft, orange; distal dendritic shaft, blue; dendritic spine, green). Three example postsynaptic targets also shown (soma, gray, distal dendrite, blue, proximal dendrite with cell body of origin, orange). (B) Quantification of synaptic targets for soma-seeded axons at P7. At least about 10% of output synapses were on identified proximal dendritic shafts [see (A)]. Seed synapse excluded for quantification of target fractions. (C) Similar analysis for apical dendrite-seeded axons at P7. Note scarcity or absence of proximal dendritic shaft and soma innervation, and substantial preference for apical dendrites and distal dendritic shafts already at P7. (D) Local connectomes between presynaptic axons [seeded from somata, apical dendrites (AD) or axon initial segments (AIS)] and their respective postsynaptic targets [other targets include dendritic spines, dendritic shafts, glia and somatic spines or filopodia, left to right, see (A) to (C)]. Each row in connectome corresponds to one axon [example in (A)], each column to one postsynaptic target; colored dots, synapses, see color bar. (E) Average conditional connectomes based on the data in (D). Data aggregated for types of axonal seed (rows) and targets (columns). Conditional probabilities *p*(*X*|*Y*) of axons innervating targets X given the axon was seeded at Y. Probabilities above 5% shown numerically (corresponding to 1 out of 20 synapses). Note signs of target preference already at P7.
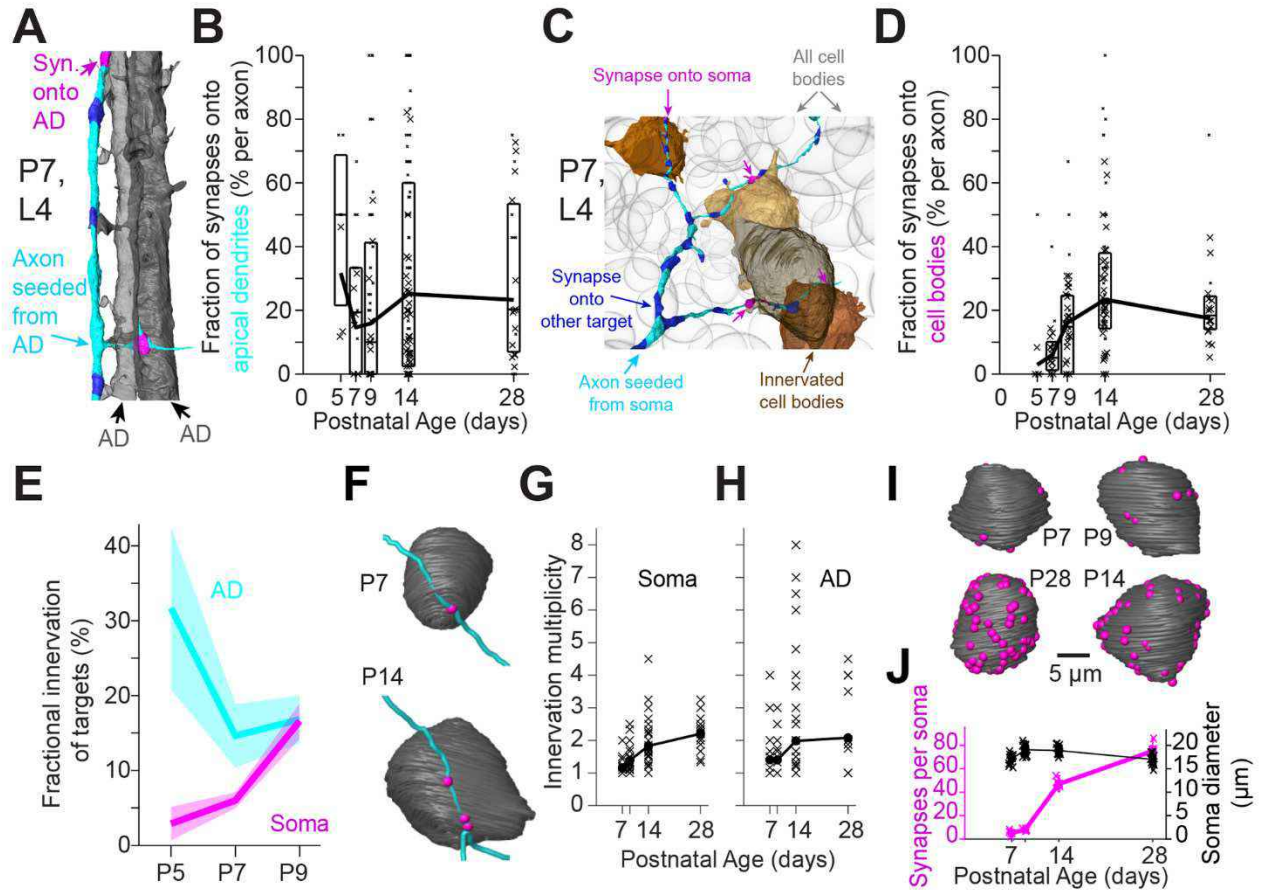
Fig. 3. Differential postnatal development of synaptic target choice by apical-dendrite- and soma-preferring axons in cortical layer 4. (**A**) Reconstruction of an axon (cyan) that was identified from its synapse (magenta) onto the shaft of an apical dendrite (AD, gray) and the other output synapses of this axon (onto other AD, magenta; onto other targets, blue) from L4 at P7. (**B**) Quantification of conditional re-innervation of apical dendrites for axons seeded at an apical dendrite. Note that conditional re-innervation of apical dendrites is at almost adult level already at P5 and P7. Number of synapses per axon: <10 (small crosses); ≥10 (large). Boxes: 25th and 75th percentile, middle line: median; thick black line: bulk fraction per age, see methods. (**C**) Reconstruction of part of an axon seeded at a soma (at P7, L4) that had 4 other synapses onto somata (magenta) and 41 onto other postsynaptic targets (blue). Branch of same axon as shown in Fig. 4C. (**D**) Fraction of synapses made again onto cell bodies for axons seeded at a soma, reported over postnatal time points [symbols as in (B)]. Note almost more than 2-fold increase of fractional soma re-innervation from P7 to P9. (**E**) Direct comparison of conditional reinnervation between P5, P7 and P9 for soma-seeded and apical dendrite (AD)–seeded axons [data from (B) and (D)]. Note difference in re-innervation rates between AD- and soma-targeting axons (shaded: SEM from bootstrapped analysis, see methods). (**F** to **H**) Development of innervation multiplicity: examples of soma-preferring axons at P7 and P14 innervating a cell body once [(F), P7, top] and three times [(E), P14, bottom]. Quantification of innervation multiplicity over postnatal time points for axons innervating somata (G) and apical dendrites (H). (**I** and **J**) Developmental increase in total number of input synapses onto cell bodies from P7 to P28. Note that soma size remains largely constant (equivalent somatic diameters shown, see methods). For statistical data, see Table 1.
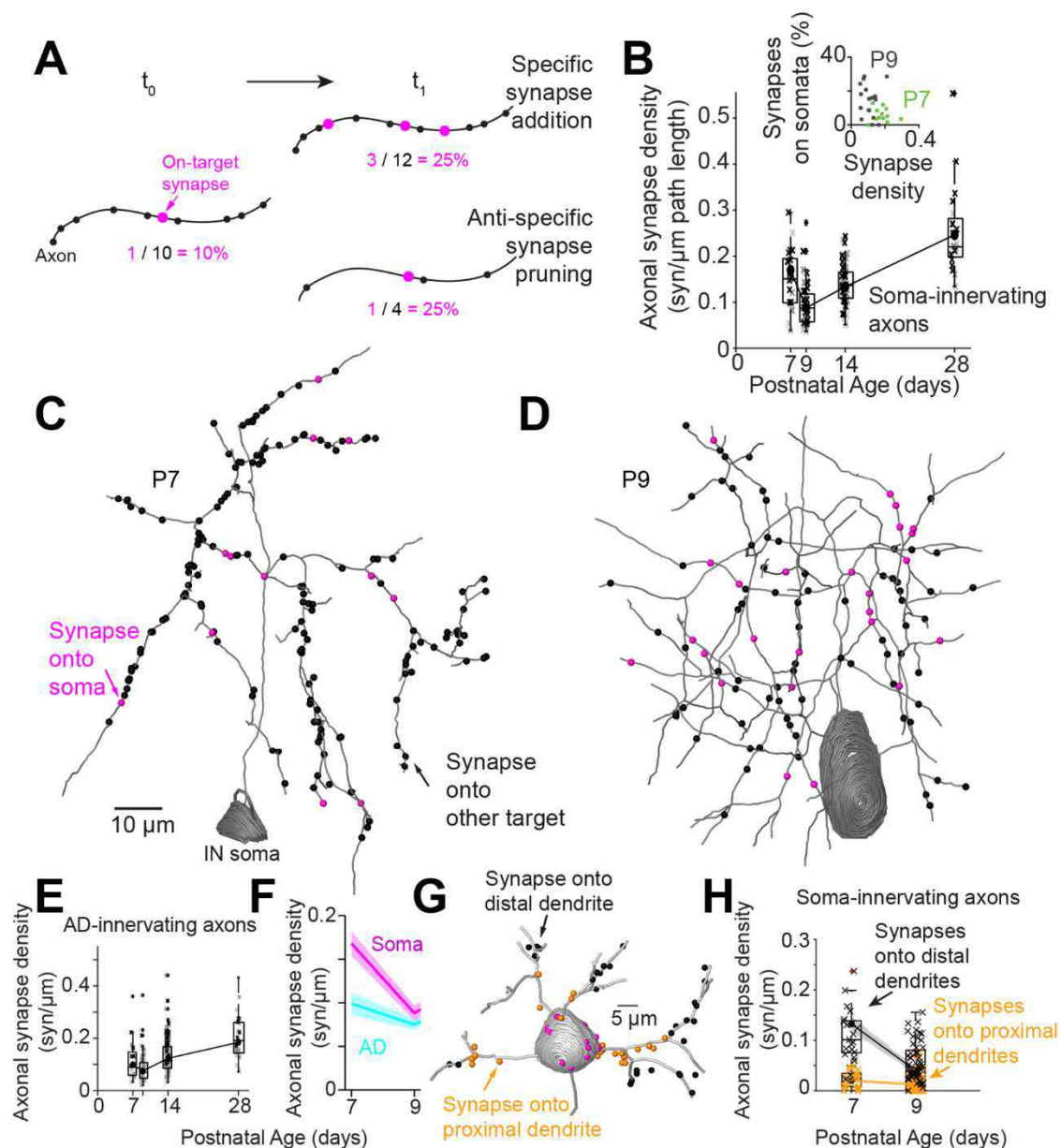
Fig. 4. Potential mechanism for development of somatic target-preference in L4. (A) Sketch of developmental processes resulting in enhanced fractional innervation of given subcellular targets over development via addition of target-specific synapses (from 1/10 synapses = 10% at time point t_0 to 3/12 synapses = 25% at time point t_1) or, alternatively, elimination of off-target synapses (from 1/10 synapses = 10% at t_0 to 1/4 synapses = 25% at t_1). Note the drop in axonal synapse density for the antispecific pruning model (bottom). **(B to D)** Quantification of axonal synapse densities of soma-preferring axons from P7 to P28 (see Table 1). Note about 2-fold drop of axonal synapse density for soma-preferring axons (B) that is clearly visible in the reconstructions [(C) and (D)]. **(E and F)** Axonal synapse density for AD-preferring axons (E) and comparison between soma- and AD-preferring axons at 7 and 9 days of age (F) indicating that the drop in synapse density is a particular phenomenon found in soma-preferring axons during the developmental phase in which somatic preference increases by more than two-fold, as predicted by the antispecific pruning model (A). See Table 1 for numbers and statistics, and fig. S4 for controls. **(G and H)** Selective maintenance of proximally but not distally placed synapses along the postsynaptic neuron: example reconstruction of postsynaptic excitatory neuron (at P9, gray) with input synapses onto soma (red), proximal (orange) and distal (black) dendrites (see methods for definition of proximal dendrites). Quantification (H) shows synapse removal is specific for those synapses made onto distal dendrites; proximally placed synapses are maintained.
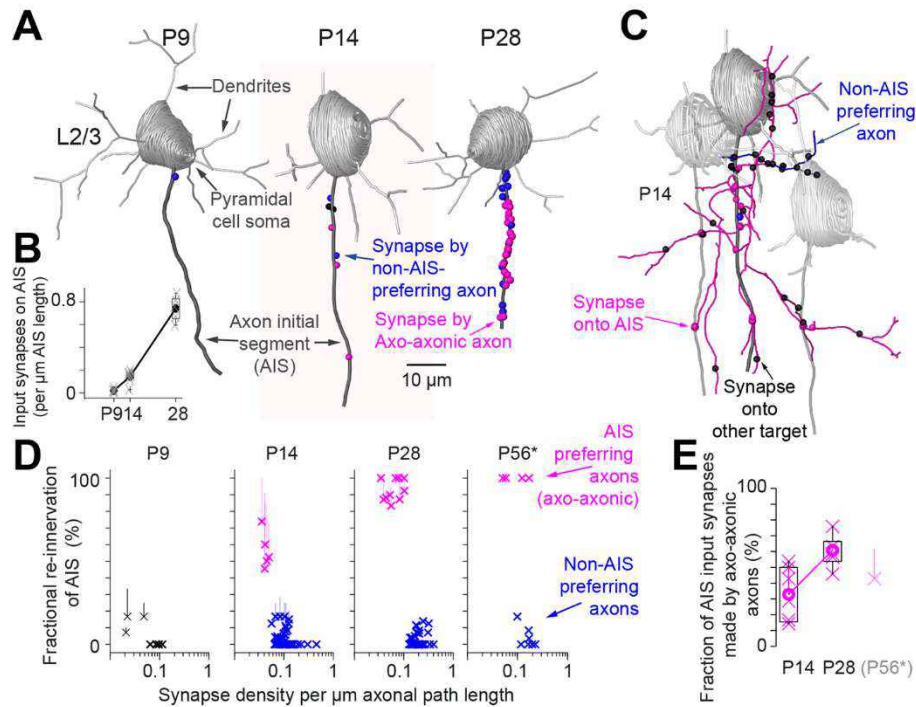
Fig. 5. Postnatal development of axon initial segment innervation in L2/3. (A) Reconstruction of L2/3 pyramidal cells from P9 to P28, their axon initial segments (AIS) and all synapses made onto these AIS. Presynaptic axons were reconstructed and identified as preferentially innervating AIS [axo-axonic axons (*18*); see (C) and (D)] or non-preferential (non-AIS preferring). (B) Development of input synapse density on AIS. (C) Illustration of axo-axonic and non-AIS preferring axons making synapses onto a given AIS. (D) Development of fractional preference for AIS innervation in a subset of axons that innervate AIS. Note that from P14 onwards, axo-axonic axons can be identified by their enhanced AIS preference (group assignment via cluster analysis, see methods; magenta: axo-axonic; blue: non-AIS preferring). Note that already from P14 onwards, off-target synapses of axo-axonic axons were noticeably smaller than those onto AIS; vertical lines indicate innervation fractions when only considering the clearest off-target synapses for quantification. *: P56 control data was analyzed in a published dataset from posterior parietal cortex (*45*). (E) Composition of input synapses onto axon initial segments (AIS): fraction of input synapses made by axo-axonic axons increases from 33–50% to 61–63% from P14 to P28 (lower bound: identified axo-axonic input axons; upper bound: 1-identified non-axo-axonic axons; difference: axons with less than 7 synapses); note that also at P56, only 43 to 63% of input synapses onto AIS were from axo-axonic axons, at least 37% from non-AIS-preferring axons (Table 1).
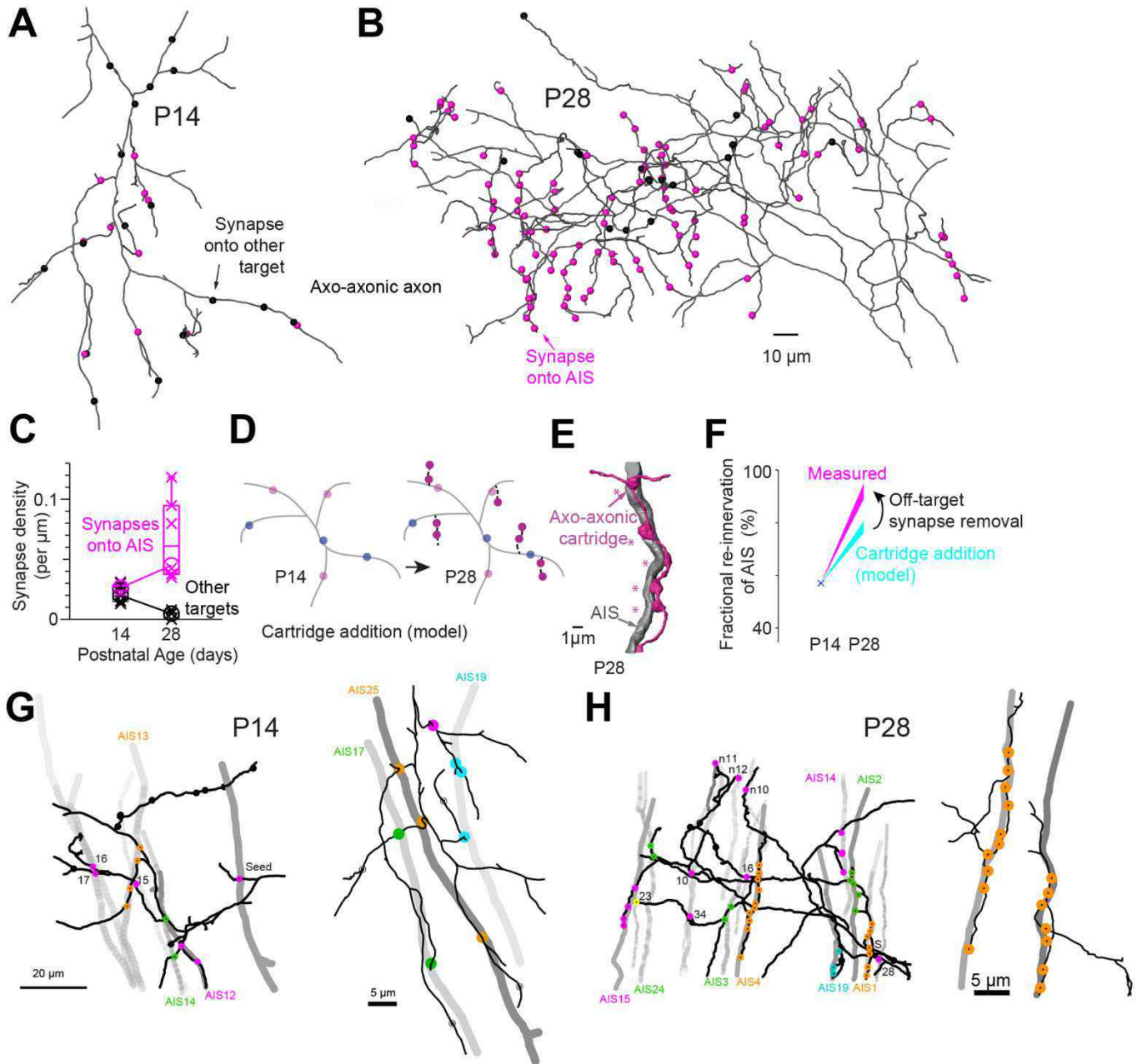
Fig. 6. Establishment of target preference in axo-axonic axons. (**A** and **B**) Example reconstructions of axo-axonic axons at P14 and P28 with all their output synapses onto axon initial segments (AIS, magenta) and other targets (black). Note paucity of vertically oriented axonal specializations ("cartridges") at P14. (**C**) While the density of synapses onto AIS increases along axo-axonic axons, synapses onto other targets decrease in density from P14 to P28. (**D** and **E**) Model for enhanced AIS-preference of axo-axonic axons at P28 via outgrowth of axon cartridges with 100% AIS preference. (**F**) Predicted (cyan) and measured (magenta) fractional AIS innervation under the model of cartridge addition with 100% AIS specificity. Model accounts for increase to 76 to 81% AIS preference; remaining reduction of off-target innervation could be accounted for by an additional pruning of 54 to 65% of off-target synapses. (**G** and **H**) Innervation of particular AIS by axo-axonic axons at P14 (G) and P28 (H) indicating that already at P14, systematic reinnervation of AIS occurs in absence of cartridges, partly by several axonal branches via en-passant synapses [right panel in (G) is part of axon shown in (A)].
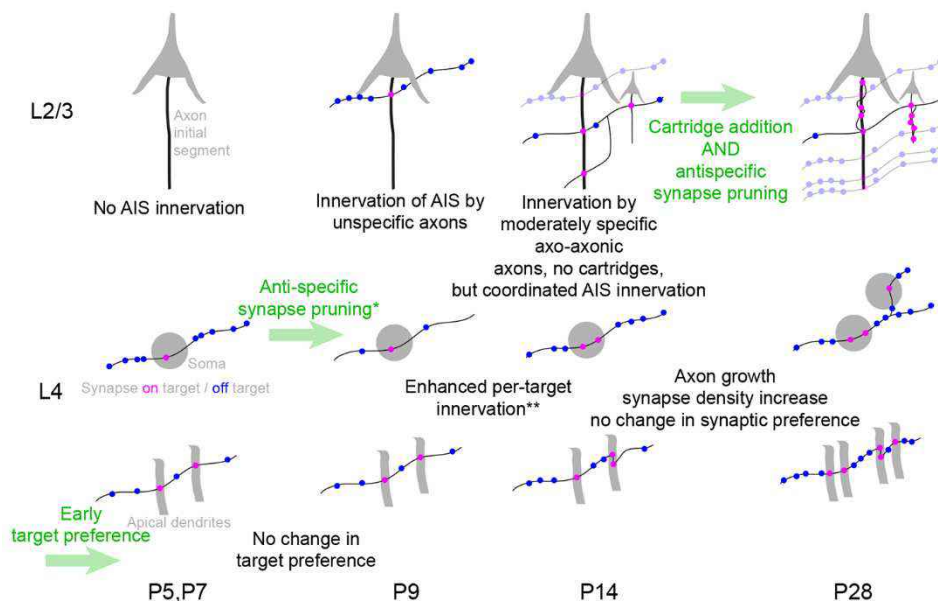
Fig. 7. Connectomic profiling of axonal target preference proposes differential developmental mechanisms for synaptic choice of somata, apical dendrites and axon initial segments. Sketch illustrating the different possible mechanisms for enhancing synaptic target preference in different classes of inhibitory axons in L2/3 and L4 between postnatal days (P) 5 and 28. *antispecific synapse pruning can account for parts but not all of preference increase (Table 1), so additional mechanisms may be at work. **Innervation multiplicity is higher for AD innervation axons than soma innervating axons already at P7, but more substantially increases after P9 (fig. S3).

Science

Postnatal connectomic development of inhibition in mouse barrel cortex

Anjali Gour, Kevin M. Boergens, Natalie Heike, Yunfeng Hua, Philip Laserstein, Kun Song and Moritz Helmstaedter

ARTICLE TOOLS	http://science.sciencemag.org/content/early/2020/12/02/science.abb4534
SUPPLEMENTARY MATERIALS	http://science.sciencemag.org/content/suppl/2020/12/02/science.abb4534.DC1
REFERENCES	This article cites 64 articles, 19 of which you can access for free http://science.sciencemag.org/content/early/2020/12/02/science.abb4534#BIBL
PERMISSIONS	http://www.sciencemag.org/help/reprints-and-permissions

Use of this article is subject to the Terms of Service